Drug Design, Development and Therapy

Dovepress
Taylor & Francis Group

Open Access Full Text Article

ORIGINAL RESEARCH

# Population Pharmacokinetic Modeling Analysis of ASC10, a Novel Antiviral Agent Targeted COVID-19, in Chinese Healthy Subjects

Duo Lv[1,2,*], Sichan Li[3,*], Yi Li[4], Meihua Lin[1,2], You Zhai[1,2], Meijia Wu[1,2], Yunqing Qiu[1,2], Qingwei Zhao[1,2], Jian Liu[1,2]

[1]Department of Clinical Pharmacy, The First Affiliated Hospital, Zhejiang University School of Medicine, Hangzhou, People's Republic of China; [2]Zhejiang Provincial Key Laboratory for Drug Evaluation and Clinical Research, Hangzhou, People's Republic of China; [3]Department of Pharmacy, Wuhan Children's Hospital (Wuhan Maternal and Child Healthcare Hospital), Tongji Medical College, Huazhong University of Science & Technology, Wuhan, People's Republic of China; [4]Institute of Antibiotics, Huashan Hospital, Fudan University, Shanghai, People's Republic of China

*These authors contributed equally to this work

Correspondence: Jian Liu, Zhejiang Provincial Key Laboratory for Drug Evaluation and Clinical Research, The First Affiliated Hospital Zhejiang University School of Medicine, Hangzhou, Zhejiang, 310003, People's Republic of China, Tel/Fax +86 571 8723 6619, Email lindaliu87@zju.edu.cn



**Background:** ASC10, an oral double prodrug of the antiviral ribonucleoside analog ASC10-A (also referred to as NHC), is currently in clinical trials for the treatment of COVID-19. Upon administration, ASC10 undergoes rapid biotransformation into the monoprodrug molnupiravir, which then swiftly converts to the active metabolite ASC10-A. Alternatively, ASC10 can directly transform into ASC10-A without forming molnupiravir as an intermediate. This study aimed to describe the population pharmacokinetics (popPK) of ASC10-A in healthy Chinese subjects and to inform clinical drug development.

**Methods:** We performed popPK modeling for ASC10-A using data from a Phase I clinical trial involving 57 healthy subjects and 1634 observations. The M3 method was employed to handle data below the quantification limit (BQL), while the Laplacian algorithm was implemented for popPK modeling. The final model was evaluated through goodness-of-fit (GOF) plots, non-parametric bootstrap method, and visual predictive check (VPC). The model-based simulations were performed to generate concentration-time profiles for ASC-10 or NHC across different studies, evaluate the exposure levels of ASC10-A under an 800 mg twice-daily dosing regimen (consistent with the recommended dose of molnupiravir), and quantify the covariate effects on the pharmacokinetic parameters of ASC10-A.

**Results:** The ASC10-A pharmacokinetics was described using a two-compartment model with first-order elimination and transit compartment absorption. Food intake and body weight were identified as influential variables on ASC10-A pharmacokinetics. The simulation results revealed that the ASC10-A exposure decreased with increasing body weight, and participants fasting could result in a higher peak concentration while retaining a similar exposure to those fed. The ASC10 dosing regimen of 800 mg every 12 hours could provide desirable exposure associated with clinical response.

**Conclusion:** This study provides a comprehensive population pharmacokinetic profile of ASC10-A in healthy Chinese volunteers. These findings support the clinical development and identification of effective regimens for ASC10.

**Keywords:** COVID-19, population pharmacokinetics, ASC10, ASC10-A, molnupiravir

## Introduction

The coronavirus disease 2019 (COVID-19) caused by the severe acute respiratory syndrome coronavirus 2 (SARS-CoV-2) constitutes an unprecedented global health crisis.[1] Since its emergence in 2019, the virus has undergone continuous mutations,[2] and its variants may compromise the effectiveness of current antiviral therapies or potentially trigger a resurgence of the pandemic. Although only a limited number of pharmacological agents have been approved for the management of COVID-19,[3] as of July 2022 just Namatevir/Ritonavir and Azvudine had received emergency conditional

Received: 17 January 2025
Accepted: 19 August 2025
Published: 26 August 2025

approval from China's National Medical Products Administration.[4] This underscores the ongoing need for development of additional therapeutics that target crucial proteins involved in the viral life cycle.[5]

ASC10 tablet is a novel therapeutic candidate currently undergoing clinical development for the treatment of COVID-19.[6] This drug is an oral prodrug of the antiviral ribonucleoside analogue β-d-n4-hydroxycytidine (ASC10-A, also referred to as NHC), which has demonstrated potential activity against influenza virus, rhinovirus, and SARS-CoV-2 in prior studies.[7] With ongoing viral evolution and emerging SARS-CoV-2 variants, ASC10-A shows promise by inhibiting multiple strains in Vero E6 cells. Advances in active pharmaceutical ingredient (API) synthesis and formulation have significantly lowered production costs, enabling rapid scale-up. These features highlight the therapeutic potential of ASC10 in addressing unmet medical needs. ASC10 undergoes rapid biotransformation to the monoprodrug molnupiravir upon administration, subsequently converting swiftly to the active metabolite ASC10-A, or directly from ASC10 to ASC10-A. The principal antiviral agent ASC10-A present in the plasma enters target organs such as the lung tissue and is further metabolized into the active triphosphate form, ASC10-A-TP. This active substance can specifically bind to the RNA-dependent RNA polymerase (RdRp), leading to significant mutations in viral RNA and a reduction in viral replication, thereby achieving a desirable antiviral effect.[8] Furthermore, the double prodrug ASC10, formed by adding a functional group to molnupiravir, exhibits optimized lipophilicity and permeability for rapid esterase-mediated activation across absorption sites, potentially enhancing active metabolite exposure and therapeutic outcomes.[6]

Bihorel et al[9] and Gouda et al[10] have characterized the population pharmacokinetics (popPK) of molnupiravir across diverse racial populations, with only Bihorel's cohort including Asians (3.6%). Their popPK models utilized a similar transit compartmental structure to depict the absorption phase of NHC, while the disposition of NHC was delineated using one-compartment and two-compartment models, respectively. The influential variables identified in their analyses predominantly encompassed sex, body size, and food status. Previous findings have revealed that the therapeutic efficacy of molnupiravir demonstrates a pronounced exposure-dependent relationship. Important exposure metrics, including the area under the concentration-time curve (AUC) and peak concentration ($C_{max}$), are closely linked to the efficacy and safety profile of molnupiravir therapy.[11] Notably, AUC over 12 hours ($AUC_{0\text{-}12}$) exhibited a strong correlation with clinical outcomes and is considered the most suitable parameter for assessing molnupiravir treatment. Previous exposure-response analyses have established that the optimal dosing regimen for molnupiravir is 800 mg administered every 12 hours, which achieves an NHC exposure level approaching the maximum therapeutic effect.[12]

Our research team previously conducted and reported the first-in-human phase I clinical trial of ASC10-A,[6] which established the pharmacokinetic basis for the current population analysis. The objectives of the current study were to characterize the population pharmacokinetic profile of ASC10-A, evaluate and quantify the influence of intrinsic factors and food status on drug exposure, and provide a crucial basis for subsequent clinical trials and pharmacokinetic-pharmacodynamic research.

# Methods

## Study Design and Population

The pharmacokinetic data set was derived from a phase I trial conducted in Chinese healthy volunteers from September 29, 2022, to December 5, 2022 (ClinicalTrials.gov: NCT05523141). This trial is comprised of two parts: a randomized, double-blind, placebo-controlled study to evaluate the safety, tolerability, and pharmacokinetics of ASC10 tablets (MAD study) and an open-label, crossover design study to evaluate food effect on the pharmacokinetics of ASC10 tablets (FE study). In the MAD study, 45 participants were administered oral doses of ASC10 ranging from 50 to 800 mg twice daily for five consecutive days and an additional dose in the morning on the sixth day. In the FE study, 12 participants received a single dose of 800 mg ASC10 either in the fasted or fed state, with at least 7 days between these two periods to permit washout.[6]

This trial was conducted in compliance with the principles of Good Clinical Practice and the Declaration of Helsinki. The study received approval from the local Ethics Committee. Written informed consents were obtained from all participants before enrollment.

## Blood Sampling and Bioanalysis

Different sampling schedules were adopted in the two parts of this phase I clinical trial. In the first part (the MAD study), pharmacokinetic blood samples were collected at pre-dose on day1, 5, and 6, at 0.25, 0.5, 1, 1.5, 2, 2.5, 3, 4, 6, 9, 12 hours post-administration of the first dose on day 1, and at 0.25, 0.5, 1, 1.5, 2, 2.5, 3, 4, 6, 9, 12, 15, 24, and 48 hours after administration on day 6. In the second part (the FE study), pharmacokinetic blood samples were collected at pre-dose, 0.25, 0.5, 1, 1.5, 2, 2.5, 3, 4, 6, 9, 12, 15, 24, 36, and 48 hours post-dose in the fasted and fed state.

The plasma concentration of ASC10-A was determined using a validated liquid chromatography-tandem mass spectrometry (UPLC-MS/MS) method in this study. The lower limit of quantification (LLOQ) for ASC10-A concentration was 10.0 ng/mL.

## PopPK Model Development

The pharmacokinetic modeling of ASC10-A concentration dataset was conducted using NONMEM (version 7.4; ICON Development Solutions, Ellicott City, MD, United States). The R program (version 4.4.0, http://www.r-project.org/) was used for statistical analysis and graphical output. The selection of a modeling algorithm should account for the proportion of data below the quantification limit (BQL) in the analytical dataset. When BQL data constitute a minor fraction (<5–10%), their influence on parameter estimates in simple models may be negligible, and exclusion (M1 method) may be justified after assessing model complexity. However, if BQL data represent a substantial proportion (>10%), initial substitution with half the LLOQ (M5 or M6 method) may be attempted. If this imputation proves insufficient, likelihood-based approaches (eg, the M3 method) should be implemented to improve parameter estimation accuracy. Among these strategies, the M3 method demonstrates optimal performance in most scenarios, particularly when BQL proportions remain below 30%. For datasets with higher BQL proportions, model simplification or alternative approaches may be necessary to ensure robust parameter estimation.[13–16]

Due to the absorption delay noted from the individual drug concentration-time profiles, the characteristics of the absorption phase were evaluated using the first-order with lag time model (LAG model), zero-order model, and transit compartment model (TRANSIT model).[17] Meanwhile, we prioritized the evaluation of one- and two-compartment structural models based on published models for NHC. While a more complex three-compartment model could be considered, the limitations of the current dataset and algorithm support precluded reliable estimation of additional parameters. For assessment of random-effects, the interindividual variabilities (IIVs) were characterized using the conventional exponential model to maintain parameter positivity; whereas residual variabilities (RVs) were tested using additive, proportional, and combined error models, with particular attention to the relationship between predicted values and residual variability patterns across these models. The base model selection process holistically considered data characteristics, diagnostic evaluations, and biological plausibility to ensure accurate representation of the pharmacokinetic profile and appropriate quantification of variability sources. This involved: (1) preliminary screening based on concentration-time profiles; (2) goodness-of-fit (GOF) diagnostic plots for model performance assessment; (3) statistical comparisons for candidate models using the objective function value (OFV) changes and the Akaike information criterion (AIC) or Bayesian information criterion (BIC) criteria; and (4) parameter precision (RSE% <30%) and condition number limits (<1000) to prevent overparameterization or model instability.[18]

After an appropriate base model was established, subject characteristics including gender, age, ethnicity, weight (WT), body mass index (BMI), and food status were investigated as potential variables. Pairwise Pearson correlation analysis was performed prior to covariate screening in order to avoid collinearity among variables incorporated in the model simultaneously. Then a stepwise approach, including both forward and backward steps, was implemented to assess the covariate effect on pharmacokinetic parameters. Criterions of a reduction of OFV by more than 3.84 ($\chi^2$ test, $P < 0.05$) and an increase of OFV by at least 6.63 ($\chi^2$ test, $P < 0.01$) were required for retention of significant covariates in the forward inclusion and backward elimination process, respectively.[19] Continuous variables were tested using power functions (equation 1) after normalization to the population median values, while categorical variables were modeled using equation 2:

$$P_i = \theta_{pop} \times \left(\frac{cov_i}{cov_m}\right)^{\theta_{cov}} \quad (1)$$

$$P_i = \theta_{pop} \times (\theta_{cov})^{covariate} \quad (2)$$

Where $\theta_{\text{pop}}$ is the population typical value of the pharmacokinetic parameters, $\theta_{\text{cov}}$ represents the influence of covariates on the parameters, $cov_{\text{i}}$ is the individual covariate value, and $cov_{\text{m}}$ is the median covariate value. The "covariate" devotes the value for a categorical variable, which is generally assigned to 0 and 1 for dichotomous variables (such as gender and food status).

## Model Evaluation

Graphical diagnosis and statistical approaches including GOF plots, non-parametric bootstrap method, and visual predictive check (VPC) were employed to evaluate the final model. Diagnostic scatter plots of population predictions (PRED) versus observations (DV), individual predicted values (IPRDE) versus DV, conditional weighted residuals (CWRES) versus PRED, and CWRES against time were depicted. The PRED-DV and IPRED-DV plots provided a visual assessment of whether the population or individual predictions adequately describe the central tendency and dispersion of the modeling data; while CWRES-PRED and CWRES-time plots further evaluate the prediction deviations to verify the accuracy and applicability of the structural model. The bootstrap procedure entailed random sampling with replacements (1000 times) from the original data to generate bootstrap data sets. The parameters with 95% confidence intervals (CIs) estimated by the bootstrap were compared to the final model estimates to assess reliability. Model robustness was further confirmed by achieving successful parameter estimation in over 80% of cases. For VPC evaluation, we simulated 1000 datasets using the final model parameters. The VPC graphs were generated for both continuous observations above the LLOQ and categorized BQL data. Specifically, for continuous observations, the median and percentile bands (eg, 5th–95th) of both observed and simulated data were calculated across time intervals. For categorical observations, the proportion of BQL observations at specific time points was computed. Model adequacy was assessed by verifying whether the observed percentiles fell within the corresponding confidence intervals of the simulated distributions.

## Model Simulation

A set of the model-derived simulations was conducted to assess the 800 mg q12h dosing regimen, which was derived from published molnupiravir study, and to explore the covariate effects on the pharmacokinetics of ASC10-A. Initially, a dosing regimen of 800 mg administered twice daily for five days was simulated for virtual subjects weighing 61.4 kg in a fasted state, serving as the reference subject for subsequent simulation analysis. The $AUC_{0\text{-}12}$ after five days of dosing was calculated through trapezoidal integration, and the $C_{max}$ and the trough concentration for each subject were also computed the minimum concentration ($C_{min}$). The rationale for the 800 mg q12h dosage in Chinese population was evaluated by comparing the exposure of ASC10-A in this study with previous findings on molnupiravir.[9] Next, the influences of significant covariates on the exposure parameters ($C_{max}$, $C_{min}$ and $AUC_{0\text{-}12}$) of ASC10-A at steady state were investigated and visualized by box plots. In this step, virtual subjects were categorized into subgroups based on essential covariates identified in the final model. For each subgroup, the ratio of predicted ASC10-A exposure under various conditions to that for the reference subjects was computed to assess the clinical significance of the important covariates. Additionally, simulations were also performed for the 800mg q12h dosing regimen of molnupiravir, generating the plasma concentration-time profile of NHC and comparing it with that of ASC10-A at the same dose.

# Results

## Demographics and Data Summary

A total of 57 subjects and 1,634 plasma concentrations of ASC10-A were included in the popPK analysis. The median age and weight of the participants were 31 (ranged 18 to 44) years and 61.4 (ranged 47.1 to 77.9) kg, respectively. The

majority of participants were of Han ethnicity, accounting for 55 individuals (96.5%). The demographic characteristics of the study cohorts are detailed in Table 1.

Overall, among the 1,634 available samples from participants, 370 concentrations were identified as BQL, which occurred mainly in the low dose group (50 mg - 200 mg) or approximately at the end of the observational period. Given that the BQL data points account for a relatively high proportion (22.6%) in the entire analytical dataset, we adopted the likelihood-based M3-method in the modeling process.[14] The BQL data was incorporated into the popPK analysis in the form of categorical observations, and the model parameters were estimated using the Laplacian algorithm.

## PopPK Model Development

Initially, visual inspection of individual concentration-time profiles revealed polyphasic disposition characteristics of ASC10-A. GOF diagnostics and statistical comparisons also confirmed that a two-compartment model provided adequate data fitting while showing significantly improved performance over a one-compartment structure. However, model expansion to three compartments led to numerically unstable parameter estimation. We therefore selected the two-compartment model to characterize the disposition of ASC10-A. The transit compartments were then incorporated into the model to describe the absorption delay. The absorption model was constructed by manual addition of transit compartments one by one, and the results revealed that including two transit compartments in the structural model was optimal. Furthermore, we tested the LAG model and zero-order model, generating simulated concentration-time curves with pharmacokinetic parameters derived from various models (Figure S1). The results demonstrated that the absorption profile was best characterized by the TRANSIT model (n = 2), which significantly improved model fit over the zero-order absorption model (ΔOFV = 29.37) and the LAG model (ΔOFV = 104.20). Thus, the selected structural model was a two-compartment model with first-order elimination and transit compartment absorption (Figure 1), which was parameterized by apparent clearance (CL), apparent volume of distribution in the central compartment ($V_C$), inter-compartment clearance (Q), apparent volume of distribution in the peripheral compartment ($V_P$), transit rate constant (KTR), and relative bioavailability (F). Additionally, the IIVs and RV were modeled using exponential functions and a combined additive and proportional error model, respectively. A combined residual error model was adopted due to the

**Table 1** Demographic Information of Enrolled Participants

| | **Part 1: Multiple Ascending Dose Study (n = 45)** | **Part 2: Food Effect Study (n = 12)** | **Total (n = 57)** |
|---|---|---|---|
| Age (years) | | | |
| Mean ± SD | 31.1 ± 7.2 | 28.0 ± 7.9 | 30.4 ± 7.4 |
| Median(Range) | 32 (18–44) | 26.5 (19–42) | 31 (18–44) |
| Sex [n (%)] | | | |
| Female | 19 (42.2) | 5 (41.7) | 24 (42.1) |
| Male | 26 (57.8) | 7 (58.3) | 33 (57.9) |
| Race [n (%)] | | | |
| Han | 43 (95.6) | 12 (100.0) | 55 (96.5) |
| Others | 2 (4.4) | 0 (0) | 2 (3.5) |
| Height (cm) | | | |
| Mean ± SD | 163.8 ± 7.7 | 165.7 ± 5.5 | 164.2 ± 7.3 |
| Median(Range) | 163.2 (148.9–180.1) | 166.6 (158.2–174.5) | 165.2 (148.9–180.1) |
| WT (kg) | | | |
| Mean ± SD | 61.5 ± 7.2 | 61.8 ± 7.5 | 61.5 ± 7.2 |
| Median(Range) | 61.1 (47.1–77.9) | 62.1 (50.4–71.2) | 61.4 (47.1–77.9) |
| BMI ($kg/m^2$) | | | |
| Mean ± SD | 22.8 ± 1.8 | 22.4 ± 2.3 | 22.8 ± 1.9 |
| Median(Range) | 23 (19–25) | 22 (19–25) | 23 (19–25) |

**Abbreviations**: SD, standard deviation; WT, body weight; BMI, body mass index.


https://doi.org/10.2147/DDDT.S517282

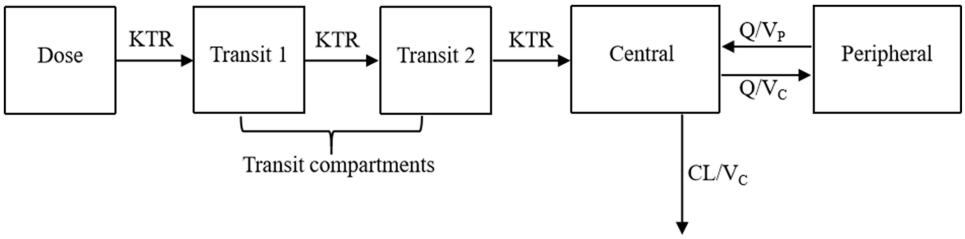


**Figure 1** Schematic representation of the popPK model for ASC10-A. A two-compartment model with first-order elimination and transit compartment absorption adequately described ASC10-A pharmacokinetics.
**Abbreviations**: KTR, transfer rate constant between transfer compartments; CL, apparent clearance; Q, inter-compartment clearance; $V_C$ and $V_P$, volume of distribution in the central and peripheral compartments, respectively.

substantial proportion of BQL data (>20%) and wide concentration range in the dataset, as neither purely additive nor proportional error models alone could adequately characterize the variability across both low and high concentrations. Implementation of alternative error models may compromise parameter estimation accuracy or lead to estimation failure.

In the covariate screening process, a significant difference in the absorption rate between subjects in the fasted and fed states was found. The inclusion of the impact of food status on KTR resulted in 213.47 drop of OFV. Then the incorporation of allometric model using WT best accounted for the effect of body size on $V_C$ (ΔOFV = 16.08) and CL (ΔOFV = 16.21). Employing BMI instead of body weight did not offer meaningful benefits to the model fit. Additionally, no effect of gender, age, or ethnicity was noted in the covariate analysis. Parameter estimates for the final model are presented in Table 2. The typical values for central CL and Vc were 79.9 L/h and 139 L, respectively, with an estimated KTR of 7.02 1/h for the absorption phase.

**Table 2** Parameter Estimates and Bootstrap Results of the Final Model

| Parameters | Final Model | | Bootstrap | | | Bias[a] (%) |
|---|---|---|---|---|---|---|
| | Estimate | RSE (%) | Median Estimate | 2.5th Percentile | 97.5th Percentile | |
| CL (L/h) | 79.7 | 2.9 | 79.54 | 75.28 | 84.39 | −0.21 |
| $V_C$(L) | 139 | 3.1 | 138.77 | 130.94 | 147.90 | −0.17 |
| Q (L/h) | 1.24 | 9.3 | 1.24 | 1.03 | 1.51 | 0.14 |
| $V_P$ (L) | 31.6 | 11.3 | 31.51 | 25.36 | 40.73 | −0.30 |
| KTR (1/h) | 7.02 | 19.5 | 6.93 | 4.87 | 10.25 | −1.31 |
| F | 1 FIX | – | – | – | – | – |
| $\theta_{CL\text{-}WT}$ | 0.903 | 21.2 | 0.89 | 0.45 | 1.25 | −1.16 |
| $\theta_{Vc\text{-}WT}$ | 1 FIX | - | - | - | - | - |
| $\theta_{KTR\text{-}food}$ | 0.474 | 16.8 | 0.48 | 0.34 | 0.65 | 1.36 |
| Interindividual variability | | | | | | |
| $\omega_{CL}$ | 17.1 | 10.6 | 16.81 | 12.67 | 20.27 | −1.70 |
| $\omega_{Vc}$ | 10.3 | 22.2 | 10.16 | 4.42 | 14.36 | −1.36 |
| $\omega_{KTR}$ | 31.9 | 9.5 | 31.61 | 25.18 | 37.60 | −0.91 |
| Residual error (proportional and additive) | | | | | | |
| $\sigma_{prop}$ | 0.41 | 5.2 | 0.41 | 0.37 | 0.45 | −0.86 |
| $\sigma_{add}$ (ng/mL) | 2.3 FIX | - | - | - | - | - |

**Notes**: [a]Bias = (median estimate from bootstrap analysis – estimate from the final model)/estimate from the final model.
**Abbreviations**: RSE, relative standard error; CL, apparent clearance; $V_C$, apparent volume of distribution in the central compartment; Q, inter-compartment clearance; $V_P$, apparent volume of distribution in the peripheral compartment; KTR, transit rate constant; F, relative bioavailability; θ, the covariate effects on parameters; ω, square root of interindividual variance for parameters; $\sigma_{prop}$, residual variability of proportional error; $\sigma_{add}$, residual variability of additive error.

## Model Evaluation

The GOF plots (Figure 2) indicated adequate model fit, with both individual and population predictions aligning well with observations. In addition, most CWRES values fell within the acceptable range of −3 to 3. According to the standard outlier detection criterion (absolute CWRES > 6),[18] no concentration data were identified as outliers or excluded from the final dataset in this analysis. Of the1000 bootstrap runs, 904 (90.4%) achieved successful minimization, with the resulting parameter estimates summarized in Table 2. The median values obtained from the bootstrap analysis closely agreed with the final model estimates, demonstrating minimal bias and thus confirming the robustness of the model. Furthermore, a graph consisting of two panels was utilized to present the VPC results for both continuous and categorical observations (Figure 3).[20] In the upper and lower panels of

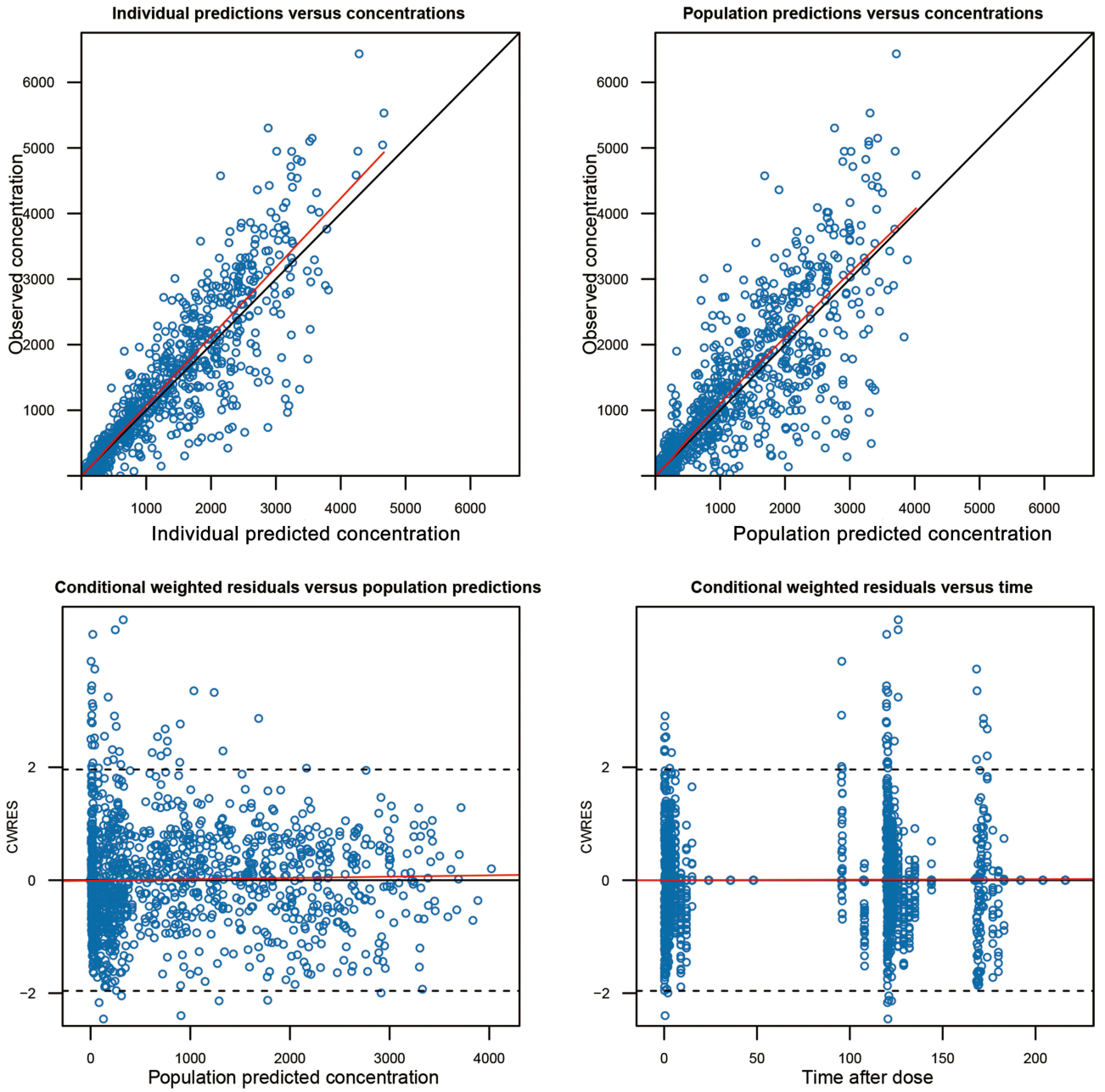


**Figure 2** Goodness-of-fit plots for the final model of ASC10-A. Blue circles are observed concentrations, black lines are reference lines, and red lines are locally weighted regression lines.


https://doi.org/10.2147/DDDT.S517282

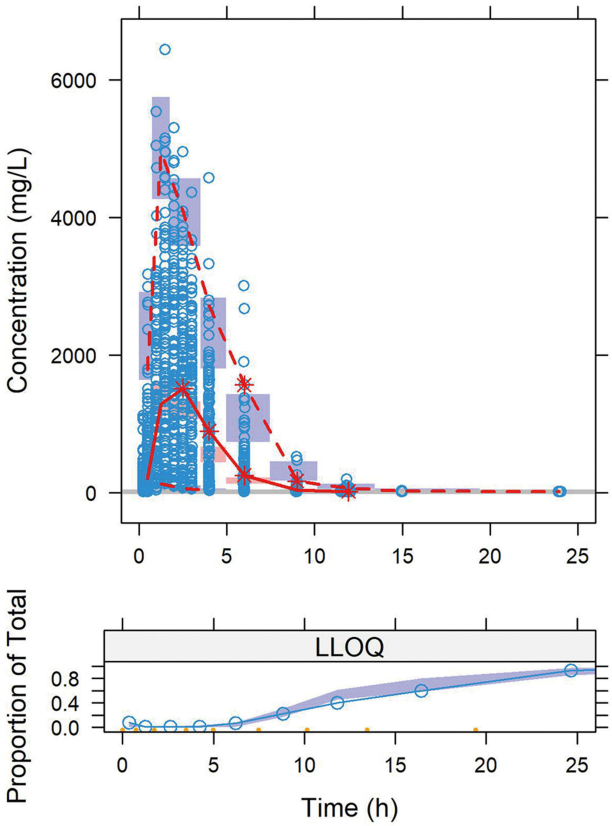


**Figure 3** Visual predictive check of the final model. In the upper panel, the open circles represent the observed data; the solid and dashed red lines represent the 5th, 50th, and 95th percentiles of observed data; the shaded area represent the 95% confidence intervals of the 5–95% simulated percentiles; the gray horizontal line is the lower limit of quantification (LLOQ) for ASC-10 (10.0 ng/mL). In the lower panel, the open circles show the fraction of observations below the LLOQ, and the shaded area is the 95% predicted intervals of simulations below the LLOQ.

the VPC plots, the percentile lines for the observations and the proportion of BQL data at each time point were superimposed with the corresponding 95% prediction intervals, suggesting satisfactory predictive performance of the final model.

## Simulation Analysis

To elucidate the differences in the absorption profiles of NHC as presented in Bihorel's study[9] and ASC10-A in our study, we depicted the steady-state concentration-time curves using simulated data derived from the final models (Figure 4). The results indicated that the peak concentration and exposure of ASC10-A in this study were lower than those of NHC in Bihorel's work, while the time to reach peak concentration for ASC10-A (1.35 h) occurred earlier than that for NHC (1.55 h).

We then evaluated ASC10-A exposure following five days of molnupiravir's recommended regimen (800 mg bid) in virtual patients weighing 61.4 kg. The geometric mean values for $C_{max}$ and AUC over 120–132 hours ($AUC_{ss}$) in these simulated patients were 3374.13 ng/mL and 10139.12 h*ng/mL, respectively.

Finally, we assessed covariate effects by comparing steady-state exposure parameters across body weight quartiles and food status categories in the simulated subjects (Figure 5). A decreasing trend in ASC10-A exposure relative to elevating patient weight was evident. The change in $AUC_{ss}$, $C_{max}$, and $C_{min}$ at steady state for subjects weighing 47.1–77.9 kg compared to the reference subjects (WT = 61.4 kg) was −20.10 to 26.77%, −20.46 to 28.57%, and −23.21 to 41.35%, respectively. Moreover, $C_{max}$ in the postprandial group was 24.02% lower than in the fasting group. However, the difference in $AUC_{ss}$ of ASC10-A between the two groups was minimal.

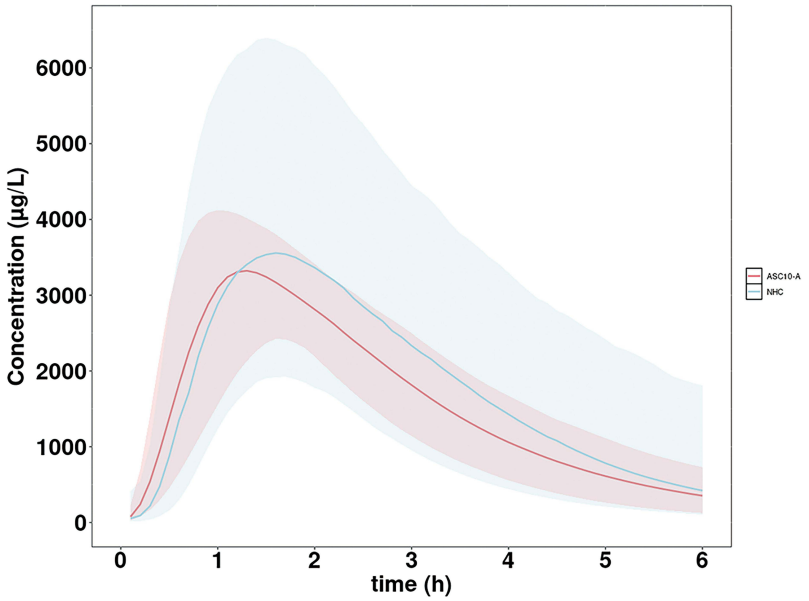


**Figure 4** Comparison of the absorption profiles of ASC10-A and NHC. The red line and blue line are the concentration-time curves for ASC10-A and NHC, respectively. The corresponding shaded area represents the variability of concentration predictions generated by the final model.

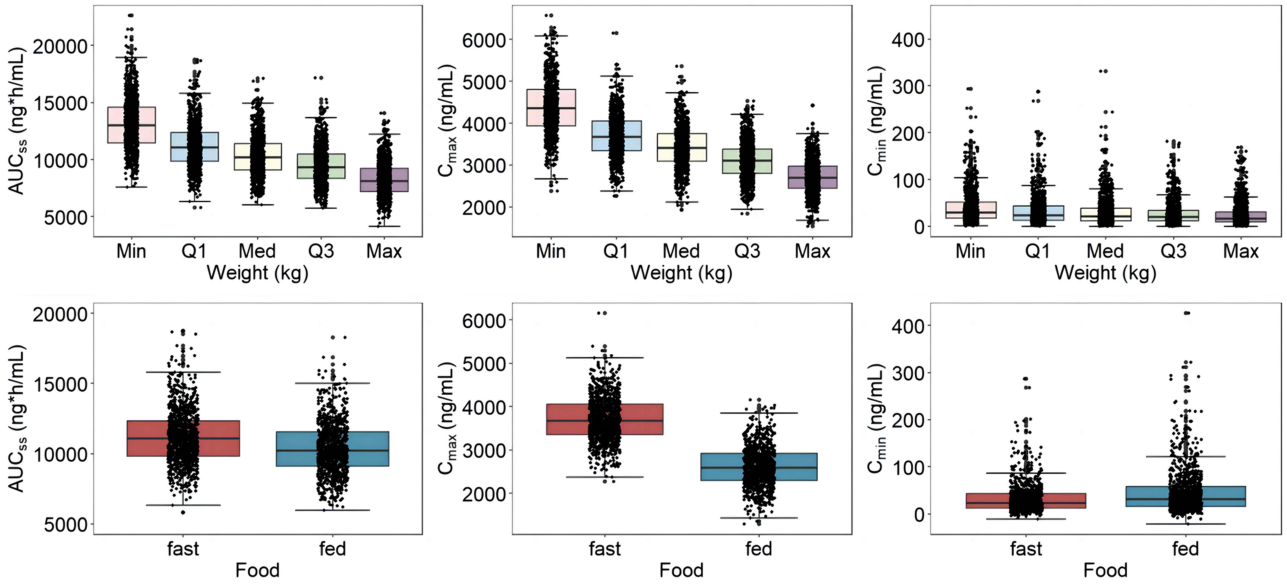


**Figure 5** The influences of body weight and food statuses on $AUC_{ss}$, $C_{max}$, and $C_{min}$.
**Abbreviations**: $AUC_{ss}$, the area under the curve (AUC) at steady state was simulated for the period of 120 to 132 hours; $C_{max}$, the peak concentration; $C_{min}$, the trough concentration; Min, minimal; Q1, the first quartile; Med, Median; Q3, the third quartile; Max, maximum.

## Discussion

The present study reported the popPK characteristics of ASC10-A, an active metabolite of ASC10, in healthy Chinese subjects for the first time. We developed a transit compartment absorption and two-compartmental disposition model with first order elimination to describe the ASC10-A pharmacokinetic profile and identify statistically significant covariate effects on pharmacokinetic parameters.

In this study, the ASC10-A clearance in the central compartment was estimated to be 1.30 L/h·kg, which is marginally greater than the NHC clearance reported by Bihorel et al, (0.88 L/h·kg)[9] and Gouda et al, (1.07 L/h·kg).[10] Both the racial differences in pharmacokinetics and the variations in sample size may explain such discrepancies. While


https://doi.org/10.2147/DDDT.S517282

the present study focused on Chinese population, Bihorel et al recruited a multiracial population with white participants predominating (66.7%), and Gouda et al exclusively studied an Egyptian cohort. Racial differences may influence drug clearance through multiple mechanisms, primarily including genetic polymorphisms, pathophysiological variations (eg, body weight and fat distribution), and environmental factors (eg, diet and concomitant medications), with genetic polymorphisms in drug-metabolizing enzymes and transporters playing a particularly crucial role.[21–23] As a structural analog of Molnupiravir, ASC10 is likely to be metabolized into its active form via esterases and amidases in the liver and intestines. Genetic variations in enzymes such as human carboxylesterase 1 (CES1), including the G143E variant (rs71647871), could significantly alter metabolic activity, as observed with drugs like oseltamivir and clopidogrel.[24] Future multicenter clinical trials evaluating the potential impact of racial differences on ASC10 pharmacokinetics would provide critical insights for global drug development and clinical dosing optimization. Regarding the absorption phase, we evaluated the fit of three common absorption models to the ASC10-A data, yielding results consistent with earlier research. When considering physiological plausibility and model performance, the transit compartment model emerged as the most appropriate one for illustrating the absorption delay in our study.[17] While the transit compartment absorption model was also employed in the studies by Bihorel et al and Gouda et al, our study incorporated a notably reduced number of NHC transit compartments (n=2) in contrast to their reported values (n=7.8 and 6). Other absorption parameters for ASC10-A also differed from previously reported NHC values. As illustrated in Figure 4, ASC10-A showed a marginally faster absorption and elimination than NHC, resulting in correspondingly lower systemic exposure and plasma concentrations. Nevertheless, ASC10-A exposure under the proposed dosing schedule remained within clinically comparable range. The observed differences may partially support the notion that ASC10's dual-pathway metabolism, combined with improved lipophilicity and permeability, contributes to its superior absorption profile.[6] Notably, the NHC concentration-time curve in Figure 4 exhibits a wider shaded area compared to ASC10. This presumably originates from the study's homogeneous data source (exclusively healthy subjects), which reduced variability in the estimated pharmacokinetic parameters and narrowed the simulated range of drug concentration variations in our model.

Since the data of this study were obtained from a relatively homogeneous group, only a limited number of variables were available for covariate analysis. Body weight, as the most common indicator of body size, was incorporated into the final model using an allometric scaling approach.[25] Two previous NHC studies similarly characterized the body weight effect on NHC clearance using allometric scaling, where the scaling factor quantitatively reflected the magnitude of clearance variation with body weight.[9,10] Simulation analyses revealed that body weight exerted a moderate effect on ASC10-A systemic exposure within the studied weight range, suggesting weight-based dose adjustment may be unnecessary. However, substantial evidence supports body weight as a critical covariate requiring dose stratification in some circumstances. A notable example comes from a popPK study of nirmatrelvir in COVID-19 patients, which demonstrated increased clearance and reduced exposure with higher body weights, necessitating individualized dosing for both underweight (<50 kg) and obese (>100 kg) patients.[26] These findings underscore the importance of collecting additional patient data for future popPK analysis to better quantify the pharmacokinetic impact of body weight on ASC10-A and establish evidence-based dosing strategies for special populations. Moreover, our study revealed that food intake significantly reduced the drug absorption rate without affecting its oral bioavailability. Although postprandial administration of ASC10 resulted in a decrease in the peak concentration and a delay in the time to peak concentration ($T_{max}$), the overall plasma exposure of ASC10-A remained unaffected by dietary conditions. Given the clinically insignificant influence of food on drug exposure, dose modification in relation to meals is unwarranted.

Additionally, the simulation results indicated that the 800 mg q12h dosing regimen for ASC10-A achieved steady-state exposure levels comparable to those reported for NHC in previous studies.[9,10] This finding could offer valuable insights for dose selection in Phase III clinical trials.[27] Nevertheless, this study has several limitations that warrant consideration. The homogeneous cohort of healthy participants may not adequately represent real-world populations with comorbidities or the target disease, potentially underestimating the IIVs in pharmacokinetic parameters. The limited sample size may also reduce statistical power for detecting clinically relevant covariate effects. Furthermore, the lack of ethnic diversity may restrict the generalizability of findings, particularly for drugs metabolized through polymorphic pathways where population genetic differences may significantly influence pharmacokinetic profiles. Finally, inherent

model assumptions might introduce additional bias. These limitations highlight the need for broader validation in diverse populations.

## Conclusion

In conclusion, we performed a popPK analysis of ASC10-A using phase I clinical trial data. The developed two-compartment model, incorporating linear first-order elimination and transit compartment absorption, adequately characterized pharmacokinetic profile of ASC10-A. While body weight and food status were identified as statistically significant covariates, their clinical relevance necessitates further prospective evaluation. Model-based simulations supported dose selection rationale for subsequent phase III trials. Furthermore, this popPK model provides a quantitative framework for future exposure-response analyses when integrated with efficacy or safety data from later-phase clinical studies.

## Abbreviations

AIC, Akaike information criterion; API, Active Pharmaceutical Ingredient; AUC, area under the plasma concentration time curve; $AUC_{0\text{-}12}$, AUC over 12 hours; BIC, Bayesian information criterion; BMI, body mass index; BQL, below the quantification limit; CIs, confidence intervals; CL, apparent clearance; $C_{max}$, peak concentration; $C_{min}$, minimum concentration; COVID-19, coronavirus disease 2019; CWRES, conditional weighted residuals; DV, observed concentration; F, bioavailability; GOF, goodness-of-fit; IIVs, interindividual variabilities; IPRDE, individual predicted values; KTR, transit rate constant; LAG, Lag time; LLOQ, lower limit of quantification; NHC, antiviral ribonucleoside analogue β-d-n4-hydroxycytidine; OFV, objective function value; popPK, population pharmacokinetic; PRED, population predictions; Q, inter-compartment clearance; RdRp, RNA-dependent RNA polymerase; RVs, residual variabilities; SARS-CoV-2, severe acute respiratory syndrome coronavirus 2; SD, standard deviation; $T_{max}$, time to peak concentration; TRANSIT, transit compartment; UPLC-MS/MS, validated liquid chromatography-tandem mass spectrometry; $V_C$, central compartment; $V_P$, peripheral compartment; VPC, visual predictive check; WT, weight.

## Data Sharing Statement

The data that support the findings of this study are available from the corresponding author upon reasonable request.

## Ethics Approval and Informed Consent

All procedures involving human participants performed in this study were approved by the Ethics Committee of the First Affiliated Hospital of Zhejiang University School of Medicine (approval No. 2022(411)) and were in accordance with the Helsinki declaration. Written informed consents were obtained from all participants before enrollment.

## Acknowledgment

We would like to thank all the healthy volunteers involved in these trials as well as the staff who contributed to this work.

## Disclosure

The authors declare that they have no competing interests.

## References

1. Yang H, Rao Z. Structural biology of SARS-CoV-2 and implications for therapeutic development. *Nat Rev Microbiol*. 2021;19(11):685–700. doi:10.1038/s41579-021-00630-8
2. Cosar B, Karagulleoglu ZY, Unal S, et al. SARS-CoV-2 mutations and their viral variants. *Cytokine Growth Factor Rev*. 2022;63:10–22. doi:10.1016/j.cytogfr.2021.06.001
3. Li G, Hilgenfeld R, Whitley R, De Clercq E. Therapeutic strategies for COVID-19: progress and lessons learned. *Nat Rev Drug Discov*. 2023;22(6):449–475. doi:10.1038/s41573-023-00672-y
4. Cao Q, Ding Y, Xu Y, et al. Small-molecule anti-COVID-19 drugs and a focus on China's homegrown mindeudesivir (VV116). *Front Med*. 2023;17(6):1068–1079. doi:10.1007/s11684-023-1037-3
5. Malone B, Urakova N, Snijder EJ, Campbell EA. Structures and functions of coronavirus replication-transcription complexes and their relevance for SARS-CoV-2 drug design. *Nat Rev Mol Cell Biol*. 2022;23(1):21–39. doi:10.1038/s41580-021-00432-z

6. Liu J, Zhao Q, Zhai Y, et al. Safety, tolerability and pharmacokinetics of ASC10, a novel oral double prodrug of a broad-spectrum antiviral agent, β-d-N4-hydroxycytidine: results from a randomized, double-blind, placebo-controlled phase 1 study in Chinese healthy subjects. *Expert Opin Invest Drugs*. 2024;33(8):867–876. doi:10.1080/13543784.2024.2377318
7. Yoon JJ, Toots M, Lee S, et al. Orally efficacious broad-spectrum ribonucleoside analog inhibitor of influenza and respiratory syncytial viruses. *Antimicrob. Agents Chemother*. 2018;62(8). doi:10.1128/aac.00766-18
8. Kabinger F, Stiller C, Schmitzová J, et al. Mechanism of molnupiravir-induced SARS-CoV-2 mutagenesis. *Nat Struct Mol Biol*. 2021;28(9):740–746. doi:10.1038/s41594-021-00651-0
9. Bihorel S, Cao Y, Chawla A, et al. Population pharmacokinetics of molnupiravir in adults with COVID-19: lack of clinically important exposure variation across individuals. *CPT*. 2023;12(12):1859–1871. doi:10.1002/psp4.13031
10. Gouda AS, Marzouk HM, Rezk MR, et al. A validated LC-MS/MS method for determination of antiviral prodrug molnupiravir in human plasma and its application for a pharmacokinetic modeling study in healthy Egyptian volunteers. *J Chromatogr B Anal Technol Biomed Life Sci*. 2022;1206:123363. doi:10.1016/j.jchromb.2022.123363
11. Painter WP, Holman W, Bush JA, et al. Human safety, tolerability, and pharmacokinetics of molnupiravir, a novel broad-spectrum oral antiviral agent with activity against SARS-CoV-2. *Antimicrob. Agents Chemother*. 2021;65(5). doi:10.1128/aac.02428-20
12. Chawla A, Birger R, Wan H, et al. Factors influencing COVID-19 risk: insights from molnupiravir exposure-response modeling of clinical outcomes. *Clin Pharmacol Ther*. 2023;113(6):1337–1345. doi:10.1002/cpt.2895
13. Jusko WJ. Use of pharmacokinetic data below lower limit of quantitation values. *Pharm Res*. 2012;29(9):2628–2631. doi:10.1007/s11095-012-0805-6
14. Ahn JE, Karlsson MO, Dunne A, Ludden TM. Likelihood based approaches to handling data below the quantification limit using NONMEM VI. *J Pharmacokinetics Pharmacodyn*. 2008;35(4):401–421. doi:10.1007/s10928-008-9094-4
15. Xu XS, Dunne A, Kimko H, Nandy P, Vermeulen A. Impact of low percentage of data below the quantification limit on parameter estimates of pharmacokinetic models. *J Pharmacokinetics Pharmacodyn*. 2011;38(4):423–432. doi:10.1007/s10928-011-9201-9
16. Hing JP, Woolfrey SG, Greenslade D, Wright PM. Analysis of toxicokinetic data using NONMEM: impact of quantification limit and replacement strategies for censored data. *J Pharmacokinetics Pharmacodyn*. 2001;28(5):465–479. doi:10.1023/a:1012247131190
17. Savic RM, Jonker DM, Kerbusch T, Karlsson MO. Implementation of a transit compartment model for describing drug absorption in pharmacokinetic studies. *J Pharmacokinetics Pharmacodyn*. 2007;34(5):711–726. doi:10.1007/s10928-007-9066-0
18. U.S. Department of Health and Human Services FaDA. Center for drug evaluation and research (CDER), center for biologics evaluation and research (CBER). population pharmacokinetics guidance for industry. Available from: https://www.fda.gov/regulatory-information/search-fda-guidance-documents/population-pharmacokinetics. Accessed August 20, 2025.
19. Sanghavi K, Ribbing J, Rogers JA, et al. Covariate modeling in pharmacometrics: general points for consideration. *CPT*. 2024;13(5):710–728. doi:10.1002/psp4.13115
20. Bergstrand M, Karlsson MO. Handling data below the limit of quantification in mixed effect models. *AAPS J*. 2009;11(2):371–380. doi:10.1208/s12248-009-9112-5
21. Chen ML. Ethnic or racial differences revisited: impact of dosage regimen and dosage form on pharmacokinetics and pharmacodynamics. *Clin Pharmacokinet*. 2006;45(10):957–964. doi:10.2165/00003088-200645100-00001
22. Johnson JA. Influence of race or ethnicity on pharmacokinetics of drugs. *J Pharm Sci*. 1997;86(12):1328–1333. doi:10.1021/js9702168
23. Ramamoorthy A, Pacanowski MA, Bull J, Zhang L. Racial/ethnic differences in drug disposition and response: review of recently approved drugs. *Clin Pharmacol Ther*. 2015;97(3):263–273. doi:10.1002/cpt.61
24. Merali Z, Ross S, Paré G. The pharmacogenetics of carboxylesterases: CES1 and CES2 genetic variants and their clinical effect. *Drug Metabol Drug Interact*. 2014;29(3):143–151. doi:10.1515/dmdi-2014-0009
25. Wang C, Peeters MY, Allegaert K, et al. A bodyweight-dependent allometric exponent for scaling clearance across the human life-span. *Pharm Res*. 2012;29(6):1570–1581. doi:10.1007/s11095-012-0668-x
26. Zhang R, Fan J, Han L, et al. Population pharmacokinetics and dosing regimen analysis of nirmatrelvir in Chinese patients with COVID-19 infection. *Drug Des Devel Ther*. 2024;18:5517–5527. doi:10.2147/dddt.S479561
27. Laffont CM, Gomeni R, Zheng B, Heidbreder C, Fudala PJ, Nasser AF. Population pharmacokinetic modeling and simulation to guide dose selection for RBP-7000, a new sustained-release formulation of risperidone. *J Clin Pharmacol*. 2015;55(1):93–103. doi:10.1002/jcph.366